

A Dynamic Control Rod Decussing Method for the 2D/1D Scheme

Ph.D. Prospectus

Aaron M. Graham

October 26, 2016

- 1 Introduction
- 2 Neutron Transport Theory
- 3 2D/1D Framework
- 4 Rod Cusping
- 5 Results
- 6 Proposed Work
- 7 Conclusions
- 8 References

Motivation

- The 2D/1D Method solves the transport equation for 3D problems
 - Faster than direct 3D transport calculations
 - More accurate than traditional nodal methods
- Control rod cusping can occur in 2D/1D
 - Occurs when control rods are partially inserted in a 2D plane
 - Causes large errors due to volume homogenization
 - Current decussing methods have trade-off between speed and accuracy
- New decussing methods are needed for 2D/1D
 - Transport-based methods that are efficient and accurate
 - New methods can reduce the computing resources required for 2D/1D
 - Other axial components (spacer grids, burnable poison inserts, axial fuel blankets, etc.) could also be simulated more efficiently using advanced decussing methods

Overview

- Implementation of sub-plane scheme
 - Captures sub-plane axial information for each 2D plane
 - Allows coarsening of axial mesh without runtime increase
- New decussing methods
 - Sub-plane scheme modified to use heterogeneous rodde/unrodde cross-sections
 - 1D Collision probabilities introduced to improve sub-plane cross-sections
- Proposed work - “sub-ray” Method of Characteristics
 - Modification to 2D MOC to resolve axial heterogeneities
 - Should resolve transport effects caused by partially inserted rods
 - Minimal runtime increase

Steady-State Multi-Group Transport Equation

$$\begin{aligned}
& \boldsymbol{\Omega} \cdot \boldsymbol{\nabla} \psi_g + \Sigma_{t,g}(\mathbf{x}) \psi_g(\mathbf{x}, \boldsymbol{\Omega}) \\
&= \frac{1}{4\pi} \sum_{g'=1}^G \int_{4\pi} \Sigma_{s,g' \rightarrow g}(\mathbf{x}, \boldsymbol{\Omega}' \rightarrow \boldsymbol{\Omega}) \psi_{g'}(\mathbf{x}, \boldsymbol{\Omega}') d\Omega' \\
&+ \frac{1}{k_{eff}} \frac{\chi_g}{4\pi} \sum_{g'=1}^G \int_{4\pi} \nu \Sigma_{f,g'}(\mathbf{x}) \psi_{g'}(\mathbf{x}, \boldsymbol{\Omega}') d\Omega' + \frac{Q_g(\mathbf{x})}{4\pi} \\
&\psi_g(\mathbf{x}_b, \boldsymbol{\Omega}) = \int_{E_n}^{E_{n-1}} \psi^b(\mathbf{x}_b, E, \boldsymbol{\Omega}) dE, \quad \boldsymbol{\Omega} \cdot \mathbf{n} < 0
\end{aligned}$$

Discrete Ordinates Approximation

- Apply quadrature to approximate integrals

$$\int_{4\pi} f(\Omega) d\Omega \approx \sum_{n=1}^N f(\Omega_n) w_n$$

- Pick a set of unique angles Ω_n

$$\begin{aligned} & \Omega_n \cdot \nabla \psi_{g,n} + \Sigma_{t,g}(\mathbf{x}) \psi_{g,n}(\mathbf{x}) \\ &= \frac{1}{4\pi} \sum_{g'=1}^G \sum_{n'=1}^N \Sigma_{g' \rightarrow g, n' \rightarrow n}(\mathbf{x}) \psi_{g',n'}(\mathbf{x}) w_{n'} \\ &+ \frac{1}{k_{\text{eff}}} \frac{\chi_g}{4\pi} \sum_{g'=1}^G \sum_{n'=1}^N \nu \Sigma_{f,g'}(\mathbf{x}) \psi_{g',n'}(\mathbf{x}) w_{n'} + \frac{Q_{g,n}(\mathbf{x})}{4\pi} \end{aligned}$$

$$\psi_{g,n}(\mathbf{x}_b) = \psi_g^b(\mathbf{x}_b, \Omega_n) \quad , \quad \Omega_n \cdot \mathbf{n} < 0$$

Transport-Corrected Scattering Approximation

- Modifies self-scatter and total cross-sections to account for anisotropy while performing isotropic calculations
- Neutron Leakage Conservation (NLC) Method: H-1

$$\Sigma_{s0,g \rightarrow g} = \Sigma_{s0,g \rightarrow g} + \frac{1}{3D_g} - \Sigma_{t,g}$$

- In-Scatter Method: B-11, C-12, O-16

$$\Sigma_{s0,g \rightarrow g} = \Sigma_{s0,g \rightarrow g} - \frac{1}{\phi_{1,g}} \sum_{g'=1}^G \Sigma_{s1,g' \rightarrow g} \phi_{1,g'}$$

- Out-Scatter Method: All other isotopes

$$\Sigma_{s0,g \rightarrow g} = \Sigma_{s0,g \rightarrow g} - \sum_{g'=1}^G \Sigma_{s1,g \rightarrow g'}$$

Diffusion Approximation

- Assumes flux is linearly anisotropic

$$\psi_g(\mathbf{x}, \boldsymbol{\Omega}) \approx \frac{1}{4\pi} (\phi_g(\mathbf{x}) + 3\boldsymbol{\Omega} \cdot \mathbf{J}_g(\mathbf{x}))$$

- Assumes relationship between scalar flux ϕ and current \mathbf{J}

$$\mathbf{J}(\mathbf{x}) \approx -\mathbf{D}(\mathbf{x}) \nabla \phi(\mathbf{x})$$

$$\mathbf{D}(\mathbf{x}) = \frac{1}{3} (\Sigma_{tr,g}(\mathbf{x}))^{-1}$$

- Eliminates angle dependence
- Simplifies streaming and scattering source terms

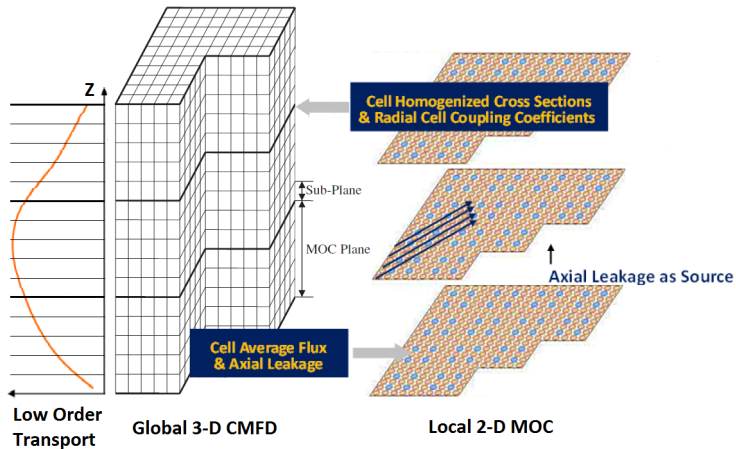
Diffusion Approximation

$$\begin{aligned}
 -\nabla \cdot \mathbf{D}_g(\mathbf{x}) \nabla \phi(\mathbf{x}) + \Sigma_{t,g}(\mathbf{x}) \phi_g(\mathbf{x}) &= \sum_{g'=1}^G \Sigma_{s0,g' \rightarrow g}(\mathbf{x}) \phi_{g'}(\mathbf{x}) \\
 + \frac{1}{k_{eff}} \frac{\chi_g}{4\pi} \sum_{g'=1}^G \nu \Sigma_{f,g'}(\mathbf{x}) \phi_{g'}(\mathbf{x}) + Q_g(\mathbf{x}) \\
 \frac{1}{4} \phi_g(\mathbf{x}_b) + \frac{\mathbf{D}_g(\mathbf{x}_b)}{2} \cdot \nabla \phi(\mathbf{x}_b) &= J_g^-(\mathbf{x}_b)
 \end{aligned}$$

Background

- Direct 3D calculations are still usually too slow for most practical calculations
- 2D/1D method was developed by researchers at Korea Atomic Energy Research Institute (KAERI) and implemented in DeCART [1, 2, 3]
 - Decomposes problem into a stack of 2D planes
 - High-fidelity transport calculations used to solve 2D planes
 - Fast 1D calculations couple 2D planes together axially
 - Reactor geometry has most of its heterogeneity in the radial direction, so lower order calculations are acceptable in axial direction
- University of Michigan (UM) developed DeCART for awhile, but decided to do a new 2D/1D implementation in MPACT [4]

Background



Radial Equations

- Average transport equation axially from $z_{k-\frac{1}{2}}$ to $z_{k+\frac{1}{2}}$
- Assume cross-sections are constant axially in region of integration

$$\Omega_x \frac{\partial \psi_g^Z}{\partial x} + \Omega_y \frac{\partial \psi_g^Z}{\partial y} + \Sigma_{tr,g}(x,y) \psi_g^Z(x,y,\Omega) = q_g^Z(x,y,\Omega) + L_g^Z(x,y,\Omega_z)$$

$$q_g^Z(x,y,\Omega) = \frac{1}{4\pi} \sum_{g'=1}^G \int_{4\pi} \Sigma_{s,g' \rightarrow g}^Z(x,y,\Omega' \cdot \Omega) \psi_{g'}^Z(x,y,\Omega') d\Omega' \\ + \frac{1}{k_{eff}} \frac{\chi_g^Z}{4\pi} \sum_{g'=1}^G \int_{4\pi} \nu \Sigma_{f,g'}^Z(x,y) \psi_{g'}^Z(x,y,\Omega') d\Omega' + \frac{Q_g^Z(x,y)}{4\pi}$$

$$L_g^Z(x,y,\Omega_z) = \frac{\Omega_z}{\Delta z_k} \left(\psi_{g,z_{k-\frac{1}{2}}} - \psi_{g,z_{k+\frac{1}{2}}} \right) \approx \frac{J_{g,z_{k-\frac{1}{2}}} - J_{g,z_{k+\frac{1}{2}}}}{4\pi \Delta z_k}$$

Axial Equations

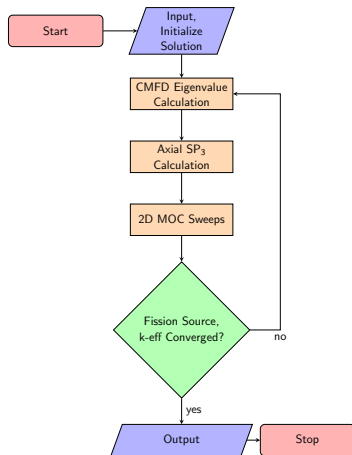
- Average transport equation over x from $x_{i-\frac{1}{2}}$ to $x_{i+\frac{1}{2}}$ and over y from $y_{j-\frac{1}{2}}$ to $y_{j+\frac{1}{2}}$
- Assume cross-sections are constant radially in region of integration

$$\Omega_z \frac{\partial \psi_g^{XY}}{\partial z} + \Sigma_{tr,g}^{XY}(z) \psi_g^{XY}(z, \Omega) = q_g^{XY}(z, \Omega) + L_g^{XY}(z, \Omega_x, \Omega_y)$$

$$L_g^{XY}(z, \Omega_x, \Omega_y) \approx \frac{J_{g,x_{i-\frac{1}{2}},y_j} - J_{g,x_{i+\frac{1}{2}},y_j}}{4\pi \Delta x_i} + \frac{J_{g,x_i,y_{j-\frac{1}{2}}} - J_{g,x_i,y_{j+\frac{1}{2}}}}{4\pi \Delta y_j}$$

Calculation Flow

- 3D CMFD [5]
 - Determines global flux shape to scale fine mesh solution
 - Calculates radial currents for 1D axial solver
- 1D NEM-SP₃ [6, 7]
 - Calculates improved axial currents for 2D solver
- 2D MOC [8, 9]
 - Solves for fine mesh scalar flux
 - Calculates updated radial currents for CMFD calculation



3D CMFD

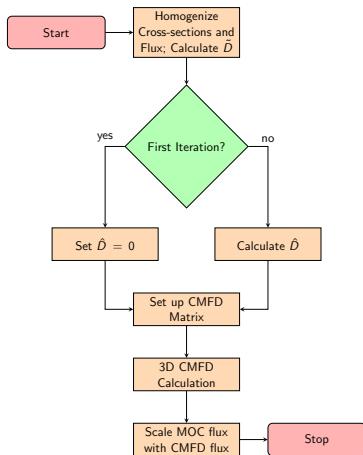
- Homogenize fine mesh flux, cross-sections, χ into coarse mesh cells
- Calculate \hat{D} coupling coefficients

$$\hat{D}_{g,s} = \frac{j_{g,s}^{MOC,k-1} + \tilde{D}_{g,s}(\phi_{g,p}^{CMFD,k} - \phi_{g,m}^{CMFD,k})}{(\phi_{g,p}^{CMFD,k} + \phi_{g,m}^{CMFD,k})}$$

- Project coarse mesh solution to fine mesh

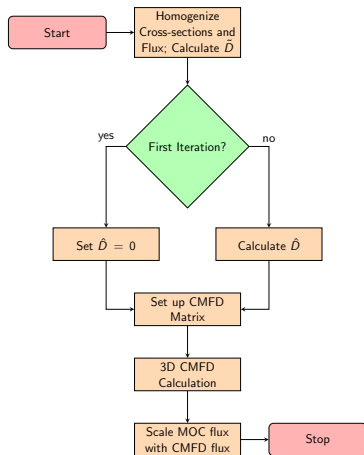
$$\phi_{g,j}^{MOC,k} = c_{g,i}^k \phi_{g,j}^{MOC,k-1}$$

$$c_{g,i}^k = \frac{\phi_{g,i}^{CMFD,k}}{\phi_{g,i}^{CMFD,k-1}}$$



3D CMFD – Sub-Plane Scheme

- Split CMFD cells axially into multiple cells
 - Calculate shaping factor for each sub-plane cell based on previous solution
 - Apply shaping factor to fine mesh fluxes during homogenization
 - Flux and ϕ have axial shape; cross-sections are axially constant
- Calculate \hat{D} for entire MOC plane; apply to all sub-planes
- Modify projection to fine mesh to account for sub-planes



1D SP₃-NEM

- SP₃ used to handle angular shape

$$\begin{aligned}
 & -\nabla \cdot D_{0,g}(\mathbf{x}) \nabla \Phi_{0,g}(\mathbf{x}) + [\Sigma_{tr,g}(\mathbf{x}) - \Sigma_{s0,g}(\mathbf{x})] \Phi_{0,g}(\mathbf{x}) \\
 & = Q_g(\mathbf{x}) + 2[\Sigma_{tr,g}(\mathbf{x}) - \Sigma_{s0,g}(\mathbf{x})] \Phi_{2,g}(\mathbf{x})
 \end{aligned}$$

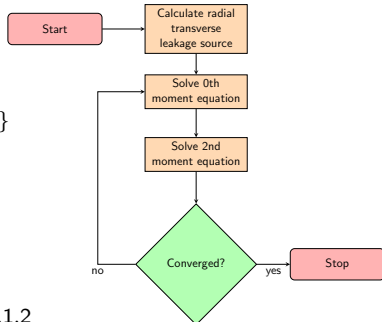
$$\begin{aligned}
 & -\nabla \cdot D_{2,g}(\mathbf{x}) \nabla \Phi_{2,g}(\mathbf{x}) + [\Sigma_{tr,g}(\mathbf{x}) - \Sigma_{s2,g}(\mathbf{x})] \Phi_{2,g}(\mathbf{x}) \\
 & = \frac{2}{5} \{ [\Sigma_{tr,g}(\mathbf{x}) - \Sigma_{s0,g}(\mathbf{x})] [\Phi_{0,g}(\mathbf{x}) - 2\Phi_{2,g}(\mathbf{x})] - Q_g(\mathbf{x}) \}
 \end{aligned}$$

- NEM used to handle spatial shape

$$Q(\xi) = \sum_{i=0}^2 q_i P_i(\xi), \quad \phi(\xi) = \sum_{i=0}^4 \phi_i P_i(\xi)$$

$$\int_{-1}^1 P_n(\xi) \left(-\frac{D}{h^2} \frac{d^2}{d\xi^2} \phi(\xi) + \Sigma_r \phi(\xi) - Q(\xi) \right) d\xi = 0, \quad n=0,1,2$$

$$\phi_L(1) = \phi_R(-1), \quad J_L(1) = J_R(-1)$$



2D MOC

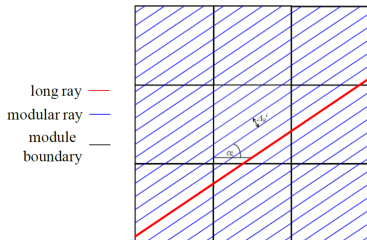
- Solve along a specific direction Ω_n

$$\mathbf{r} = \mathbf{r}_0 + s\Omega_n \Rightarrow \begin{cases} x(s) = x_0 + s\Omega_{n,x} \\ y(s) = y_0 + s\Omega_{n,y} \\ z(s) = z_0 + s\Omega_{n,z} \end{cases}$$

- Problem reduces from PDE to ODE that can be solved analytically

$$\frac{\partial \psi_{g,n}}{\partial s} + \Sigma_{t,g}(\mathbf{r}_0 + s\Omega_n) \psi_{g,n}(\mathbf{r}_0 + s\Omega_n) = q_{g,n}(\mathbf{r}_0 + s\Omega_n)$$

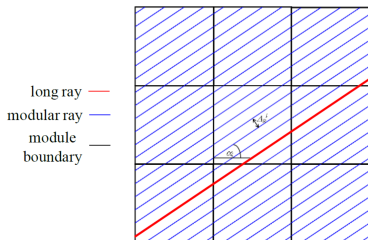
$$\begin{aligned} \psi_{g,n}(\mathbf{r}_0 + s\Omega_n) &= \psi_{g,n}(\mathbf{r}_0) \exp\left(-\int_0^s \Sigma_{t,g}(\mathbf{r}_0 + s'\Omega_n) ds'\right) \\ &+ \int_0^s q_{g,n}(\mathbf{r}_0 + s'\Omega_n) \exp\left(-\int_0^{s'} \Sigma_{t,g}(\mathbf{r}_0 + s''\Omega_n) ds''\right) ds' \end{aligned}$$



2D MOC

- Assume flat source, cross-section along track with length L_j and spacing δx

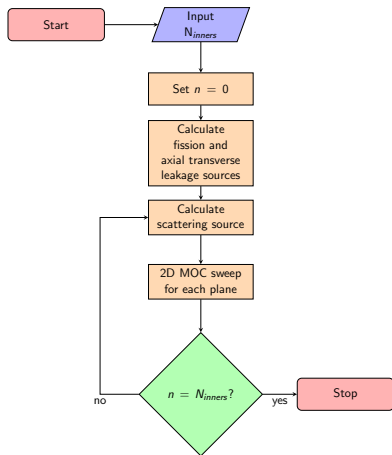
$$\begin{aligned}\psi_{out,g,i,n,j} &= \psi_{in,g,i,n,j} e^{-\Sigma_{t,g,i} L_j} \\ &\quad + \frac{q_{g,i,n}}{\Sigma_{t,g,i}} \left(1 - e^{-\Sigma_{t,g,i} L_j} \right) \\ \bar{\psi}_{g,i,n,j} &= \frac{q_{g,n,i}}{\Sigma_{t,g,i}} \\ &\quad + \frac{1 - e^{-\Sigma_{t,g,i} L_j}}{L_j \Sigma_{t,g,i}} \left(\psi_{in,g,i,n,j} - \frac{q_{g,n,i}}{\Sigma_{t,g,i}} \right) \\ \bar{\psi}_{g,i,n} &= \frac{\sum_j \bar{\psi}_{g,i,n,j} \delta x A_j}{\sum_j \delta x A_j}\end{aligned}$$



- Modular ray tracing can be used to minimize storage requirements by tracing only portions of problem geometry

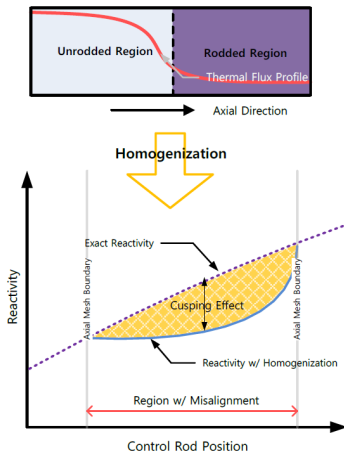
2D MOC

- Perform ray tracing and store segment information up front
- Set up scattering, fission, and axial transverse leakage sources
 - 1-group sweeping
 - Multi-group sweeping
- Parallel Decomposition
 - Spatial (Planar and Radial)- MPI
 - Angle - MPI
 - Ray - OpenMP



Background

- Nodes must be axially homogeneous
- Control rod positions often do not align with node boundaries, requiring homogenization of control rod and moderator
- Volume homogenization preserves material volume/mass, but not reaction rates
- Two approaches to prevent rod cusping:
 - Refine mesh to align with all control rod positions
 - Decusping method to improve homogenization



2D/1D Decusping Methods

- Neighbor Spectral Index Method - CRX-2K [10]
 - Spectral index is defined as the ratio of the fast flux to the thermal flux
 - Spectral index is used in top and bottom neighbor nodes to estimate partially rodded node flux profile
 - This estimate is used to update cross-sections each iteration
- nTRACER Method [11]
 - Solves local problem to generate CMFD constants
 - Performs CMFD calculations on fine mesh to obtain axial flux profiles
 - Uses axial flux profiles during full core calculation to homogenize cross-sections
- Polynomial decusping - MPACT [12]
 - A series of 3x3 assembly cases were run with partially rodded nodes in the center assembly
 - Results were used to generate polynomials of decusping error as function of rod insertion
 - Polynomials are used to reduce the control rod volume fraction when homogenizing

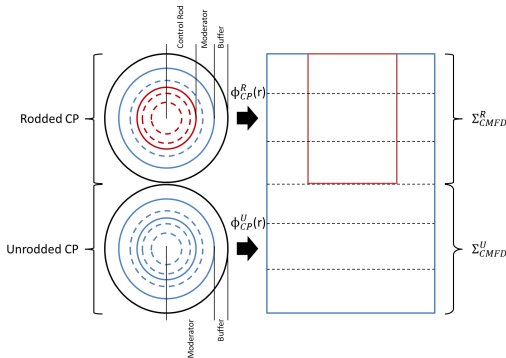
Sub-Plane Decusping

- Modifications made to sub-plane scheme to treat axial effects of rod cusping
 - Homogenization still uses MOC flux with axial shape factor, but with heterogeneous rodded or unrodded cross-sections
 - Projection re-homogenizes cross-sections in partially rodded nodes after CMFD calculation

$$\overline{\Sigma}_i = \frac{\phi_{rad,i}^R \phi_{ax,i}^R \Sigma_i^R h^R + \phi_{rad,i}^U \phi_{ax,i}^U \Sigma_i^U h^U}{\phi_{rad,i}^R \phi_{ax,i}^R h^R + \phi_{rad,i}^U \phi_{ax,i}^U h^U}$$

Collision Probabilities Decusping

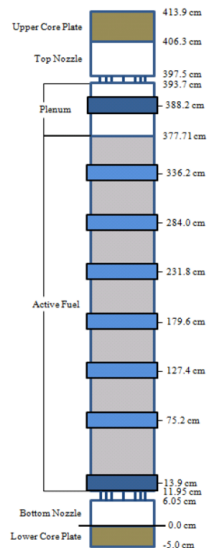
- Sub-plane modifications only capture axial effects
 - MOC uses homogenized cross-section
 - Radial shape does not accurately reflect either region
- 1D collision probabilities (CP) introduced to generate radial shapes
 - Generates radial flux profile for rodDED and unroDED region
 - Radial profiles used in CMFD homogenization
 - Very efficient calculation



VERA Problem 4

- Center 3x3 assembly cluster in Watts Bar Unit 1
- AIC Control rod in center assembly placed at 257.9 cm
- Test cases used 57 planes, with rod inserted 50% into a plane
- Reference used 58 planes, with extra plane boundary aligned with rod tip
- All simulations used 1 core per plane

2.1	2.6 20 PY	2.1
2.6 20 PY	2.1 RCCA	2.6 20 PY
2.1	2.6 20 PY	2.1



Problem 4 Results

Case	k-eff Difference (pcm)	Pin Power Differences		Iterations		Runtime (Core-Hours)
		RMS	Max	2D/1D	CMFD	
Reference	–	–	–	12	364	8.59
No Treatment	-30	3.84%	21.81%	12	352	9.23
Polynomial	-8	1.03%	6.58%	12	360	9.50
Sub-plane	-7	1.13%	7.11%	12	409	9.26
Sub-plane + 1D-CP	-2	0.54%	4.94%	12	364	9.45

VERA Problem 5

- Bank D inserted to 257.9 cm, other banks all out
- 57 planes for tests and 58 for reference, 16 cores per plane

	H	G	F	E	D	C	B	A
8	2.1 20	2.6 20	2.1 20	2.6 20	2.1 20	2.6 20	2.1 20	3.1 12
9	2.6 20	2.1 24	2.6 24	2.1 20	2.6 20	2.1 24	3.1 24	3.1
10	2.1 24	2.6 24	2.1 20	2.6 20	2.1 16	2.6 16	3.1 8	3.1
11	2.6 20	2.1 20	2.6 20	2.1 20	2.6 20	2.1 16	3.1 16	3.1
12	2.1 20	2.6 20	2.1 20	2.6 20	2.6 24	3.1		
13	2.6 20	2.1 16	2.6 24	2.1 12	3.1	3.1		
14	2.1 24	3.1 16	2.1 16	3.1	3.1	3.1		
15	3.1 12	3.1 8	3.1	3.1	Enrichment Number of Pyrex Rods			

	H	G	F	E	D	C	B	A
8	D		A		D		C	
9						SB		
10	A		C				B	
11				A		SC		
12	D				D		SA	
13		SB		SD				
14	C		B		SA			
15								

Problem 5 Results

Case	k-eff Difference (pcm)	Pin Power Differences		Iterations		Runtime (Core-Hours)
		RMS	Max	2D/1D	CMFD	
Reference	–	–	–	13	481	362
No Treatment	-22	6.90%	30.55%	13	523	411
Polynomial	-5	1.15%	4.85%	13	463	374
Sub-plane	-5	2.09%	10.20%	13	499	399
Sub-plane + 1D-CP	-1	0.50%	2.74%	13	529	426

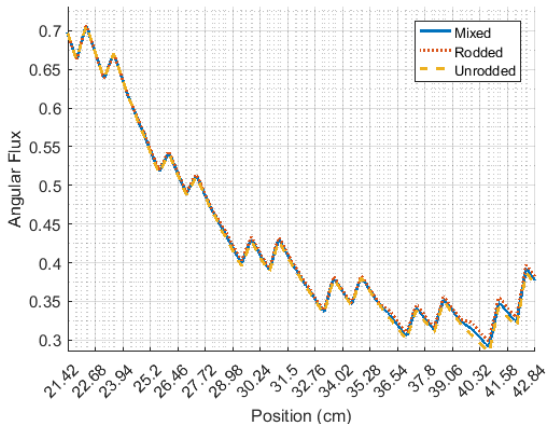
1D MOC Code

- A transport-based solution that resolves decussing directly with MOC is desired
- To aid in developing this method, a 1D MOC code was written
 - Able to visualize and analyze angular flux
 - Simulations with mixed roddeed/unroddeed cross-sections
 - Can perform fixed source (fission or total) and eigenvalue calculations
- Results provide insights into effects of rod cusping on angular flux

Fixed Total Source

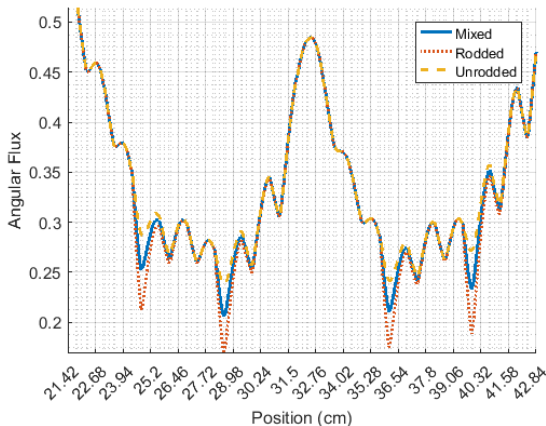
- 1D model of VERA Problem 4
 - Center row across all 3 assemblies (51 pin cells)
 - center assembly has 4 partially rodged positions
 - C5G7 cross-sections [13, 14]
- Eigenvalue calculation performed to generate fission and scattering source distributions
- MOC sweeps used this source for 0%, 50%, and 100% rodged cross-sections

Fixed Total Source



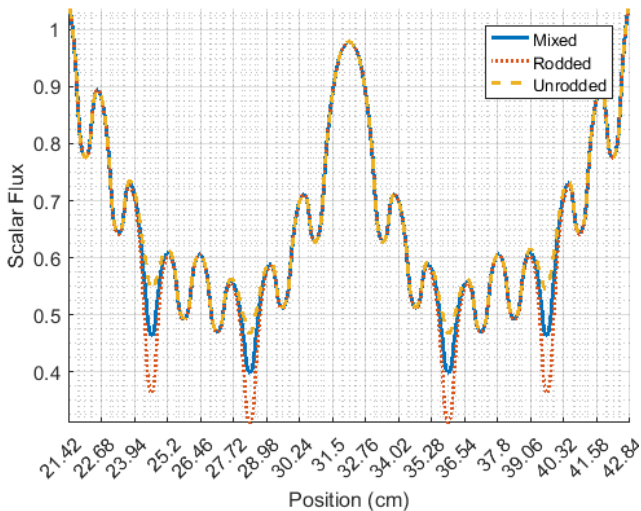
- Fast flux differences are small but build up

Fixed Total Source



- Thermal flux differences are large but dissipate quickly

Fixed Total Source

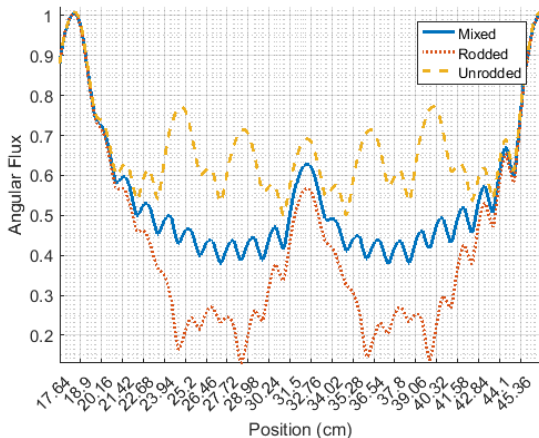


Fixed Fission Source

- 1D model of VERA Problem 4
- Eigenvalue calculation performed to generate fission source
- Calculations performed using 25%, 50%, and 75% rodged cross-sections
 - Same, fixed fission source for each case
 - Multiple iterations allowed for each case to converge scattering source

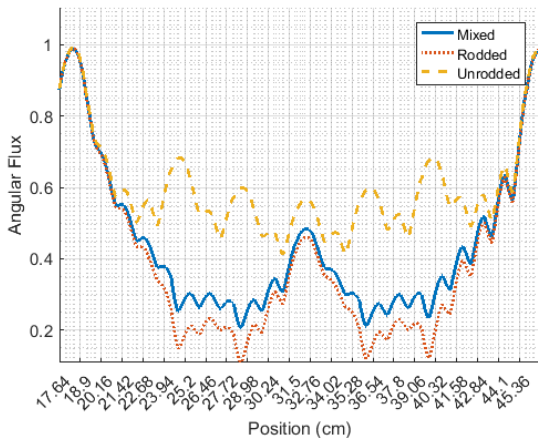
Fixed Fission Source

- Angular Flux, Group 7, 25% rodded



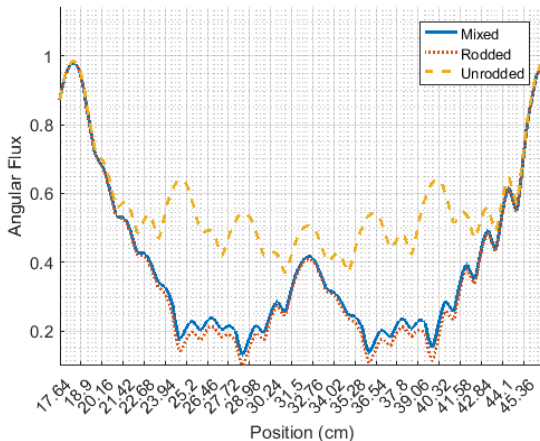
Fixed Fission Source

- Angular Flux, Group 7, 50% rodded



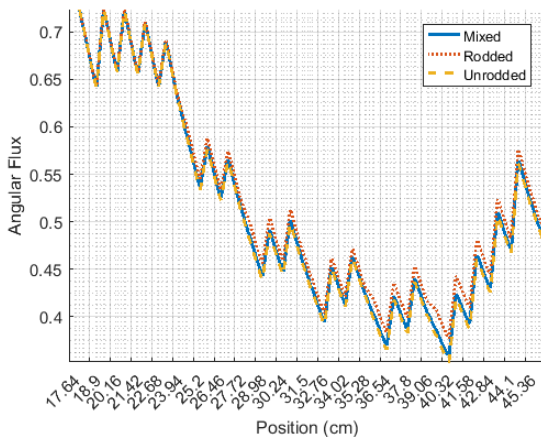
Fixed Fission Source

- Angular Flux, Group 7, 75% rodded



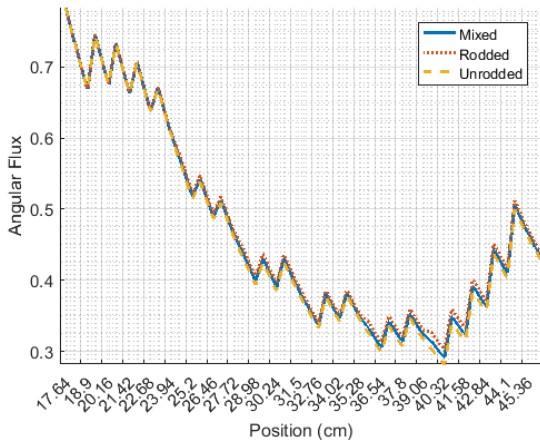
Fixed Fission Source

- Angular Flux, Group 1, 25% rodded



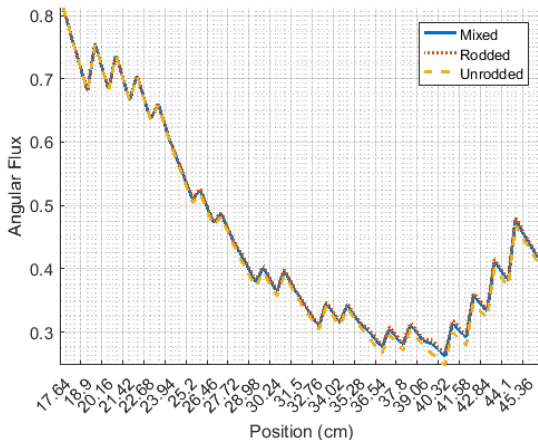
Fixed Fission Source

- Angular Flux, Group 1, 50% rodded



Fixed Fission Source

- Angular Flux, Group 1, 75% rodded



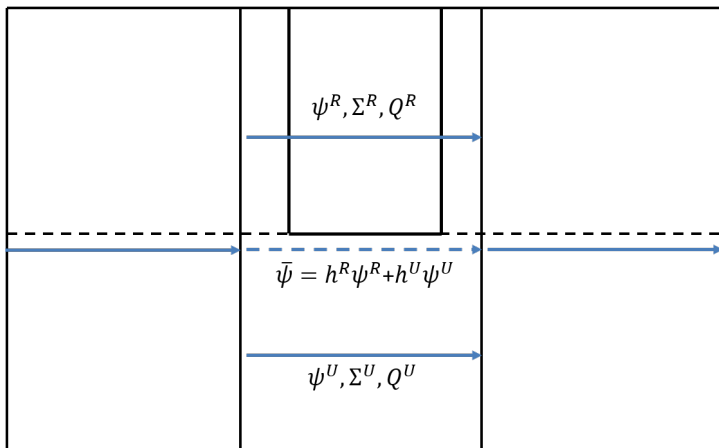
1D MOC Summary

- Fixed total source
 - Differences between rodded and unrodded thermal flux are only significant in partially rodded cell
 - Fast fluxes differences are small, but last much longer
- Fixed fission source
 - Scattering source in neighboring pins changes significantly depending on partially rodded cell
 - If angular flux exiting partially rodded cells is treated, neighboring pin cells will not be affected by cusping
 - Need to capture difference between rodded and unrodded angular flux

Sub-Ray MOC Method

- Perform standard 2D MOC calculations in pin cells with no cusping effects
- For partially rodged pin cells, use multiple “sub-rays” to capture partially rodged effects
 - Use sub-planes to determine sources for rodged and unrodged regions
 - Determine angular flux with rodged cross-section and source; repeat with unrodged values
 - Average rodged and unrodged angular flux for each ray segment
- Angular flux exiting pin cell will prevent cusping effects in neighboring cells
- Currents used for sub-plane CMFD \hat{D} can be calculated using explicit rodged and unrodged angular fluxes
- Sub-rays could be used for other reactor components such as spacer grids, burnable poison inserts, etc.

Sub-Ray MOC Method



Conclusions

- Rod cusping problem explained and demonstrated
- New decusping methods developed
 - Improved accuracy over previous methods
 - Minimal runtime increases
 - Still room for improvement
- 1D MOC results showed effects of volume homogenization on angular flux
- Sub-ray MOC method development motivated by current decusping methods and 1D MOC results

Next Steps

Task	Description	Target Date
1	Analysis of cross-section and source effects on angular flux	10/2016
2	Development of sub-ray MOC method	12/2016
3	Prototype of method in 1D MOC code	03/2017
4	Implementation of method in MPACT	06/2017
5	Testing on VERA Problem 4, 5, 9, and transient test problem	08/2017

Acknowledgments

- This material is based upon work supported under an Integrated University Program Graduate Fellowship.
- This research was supported by the Consortium for Advanced Simulation of Light Water Reactors (www.casl.gov), an Energy Innovation Hub (<http://www.energy.gov/hubs>) for Modeling and Simulation of Nuclear Reactors under U.S. Department of Energy Contract No. DE-AC05-00OR22725.
- This research also made use of resources of the Oak Ridge Leadership Computing Facility at the Oak Ridge National Laboratory, which is supported by the Office of Science of the U.S. Department of Energy under Contract No. DE-AC05-00OR22725.
- This research made use of the resources of the High Performance Computing Center at Idaho National Laboratory, which is supported by the Office of Nuclear Energy of the U.S. Department of Energy under Contract No. DE-AC07-05ID14517.



J. Y. Cho *et al.*

“Three-dimensional heterogeneous whole core transport calculations employing planar moc solutions.”

In: *Trans. Am. Nucl. Soc.*, volume 87, (pp. 234–236) (2002).



M. Hursin, B. Kochunas, and T. Downar.

DeCART Theory Manual.

Technical report, University of Michigan (2008).



H. G. Joo *et al.*

“Methods and performance of a three-dimensional whole-core transport code decart.”

In: *PHYSOR 2004 – The Physics of Fuel Cycles and Advanced Nuclear Systems: Global Developments*. Chicago, Illinois (2004).



MPACT Team.

MPACT Theory Manual.

Technical report, Oak Ridge National Laboratory and the University of Michigan (2015).



K. Smith.

“Nodal method storage reduction by nonlinear iteration.”

Trans. Am. Nucl. Soc., **44**: p. 265 (1983).



R. G. McClarren.

“Theoretical aspects of the simplified pn equations.”

Transport Theory and Statistical Physics, **39(2-4)**: pp. 73–109 (2011).



H. Finnemann, F. Bennewitz, and M. Wagner.

“Interface current techniques for multidimensional reactor calculations.”

Atomkernenergie, **30(2)**: pp. 123–128 (1977).



J. Askew.

A characteristics formulation of the neutron transport equation in complicated geometries.

Technical report, United Kingdom Atomic Energy Authority (1972).



M. Halsall.

CACTUS, a characteristics solution to the neutron transport equations in complicated geometries.

Technical report, UKAEA Atomic Energy Establishment (1980).



B. Cho and N. Z. Cho.

“A nonoverlapping local/global iterative method with 2-d/1-d fusion transport kernel and p-cmfd wrapper for transient reactor analysis.”

Annals of Nuclear Energy, **85**: pp. 937–957 (2015).



Y. S. Jung and H. G. Joo.

“Control rod decussing treatment based on local 3-d cmfd calculation for direct whole core transport solvers.”

In: *Proceedings of the International Congress on Advances in Nuclear Power Plants (ICAPP)* (2014).



B. M. Kochunas *et al.*

“VERA core simulator methodology for pwr cycle depletion.”

In: *Proceedings of the ANS Joint International Conference on Mathematics and Computation (M&C 2015), Supercomputing in Nuclear Applications (SNA), and the Monte Carlo (MC) Method*. Nashville, TN, USA.

URL <http://www.cas1.gov/docs/CASL-U-2015-0155-000.pdf> (2015).



E. E. Lewis *et al.*

Benchmark on Deterministic Transport Calculations without Spatial Homogenization.

Technical report, Nuclear Energy Agency Organisation for Economic Cooperation and Development (NEA-OECD) (2003).



E. E. Lewis *et al.*

Benchmark on Deterministic Transport Calculations without Spatial Homogenization: MOX Fuel Assembly 3-D Extension Case.

Technical report, Nuclear Energy Agency Organisation for Economic Cooperation and Development (NEA-OECD) (2005).